PHYSICAL REVIEW B VOLUME 38, NUMBER 2 15 JULY 1988-I

Transient-photomodulation-spectroscopy studies of carrier thermalization and recombination in *a*-Si:H

H. A. Stoddart, Z. Vardeny,* and J. Tauc
Department of Physics and Division of Engineering, Brown University, Providence, Rhode Island 02912
(Received 12 November 1987)

The transient response of mid-gap absorption in *a*-Si:H to pulsed optical excitation is studied as a function of time (300 ns to 30 ms) and sample temperature (10–220 K) with use of probe wavelengths ranging from 0.75 to 5.5 μm. A numerical inversion process applied to the data gives the distribution of excess carriers in both energy and time. Analytical and numerical results describing the thermalization of carriers in an exponential bandtail have been obtained which agree well with the data. A detailed recombination model which includes both carrier release from the demarcation energy and direct tunneling to recombination centers is discussed in association with the experimental results along with a comparative analysis of spectrally resolved transient-photoluminescence decays.

I. INTRODUCTION

The nature and density of states (DOS) in the gap of an amorphous semiconductor determine the suitability of the material as an optoelectronic device. The main reason for this is that the gap states, acting as traps and recombination centers, determine the relaxation processes of photogenerated carriers. Conventional methods used for studying these processes are time-resolved photoluminescence (PL),[1,2] photoconductivity (PC),[3–5] and light-induced electron-spin resonance.[6] Photoluminescence monitors a subset of transitions that are radiative, PC follows a subset of photocarriers which have an appreciable mobility, and from LESR one can learn about the photoinduced changes in the densities of singly occupied electron states. Although the technique of photomodulation (PM) on which our work is based has not been utilized as extensively as these methods,[7] it does provide information not otherwise obtainable.[8] Steady-state photomodulation spectroscopy, for example, gives the transition energies involving states in the gap. When pulsed excitation is applied, one can additionally study the time evolution of the total oscillator strength of the bands and relate it to carrier thermalization and recombination processes.

We have improved PM measurements by incorporating into a single experiment both time and energy resolution which we have used to obtain detailed information about carriers trapped with the gap of a Si:H. As in the transient PM experiment,[9] carriers are optically excited using a pulsed laser. After subsequent trapping in gap states, the carriers undergo a sequence of thermalization and recombination steps. Detection of the number of trapped carriers is accomplished by the use of a second (probe) beam which measures the induced change in transmission (ΔT). As in the steady-state experiment,[10] information pertaining to the location of the carriers in energy is obtained from the spectral resolution of $\Delta T/T$. We observe both shallow and deep trapped carriers with differing time dependences.

Due to the wealth of data this experiment provides, existing models of carrier dynamics proved to be too restrictive to account for all our results although adequate agreement to various features of the data were obtained over limited ranges of sample temperature. For example, above 100 K, the multiple trapping model[11,12] describes the time dependence of total carrier recombination from the bandtail. At lower temperatures, tunneling models[13,14] provide reasonably accurate fits to the total decay as well as to the shape of the distribution of carriers.

Motivated by these results and guided by the work of Monroe,[13] we have pursued a theoretical analysis which treats tunneling and thermally activated hopping as competing processes in a single unified model. The solutions obtained are based on simple assumptions and depend only on material parameters. Excellent agreement to all the features of the data is obtained and the deduced material parameters match values reported elsewhere. Some interesting conclusions pertaining to the influence of defects on recombination have been drawn. A comparative analysis of spectrally resolved transient-photoluminescence data acquired under the same conditions as the PM data provides valuable independent verification of our conclusions. In particular, this data proves that recombination between bandtails is dominated by transitions through defects rather than by direct tunneling.

The paper is organized as follows. Section II deals with the apparatus. Experimental results and their preliminary analysis are presented in Secs. III and IV. A theoretical description of carrier kinetics based on hopping in exponential bandtails is given in Sec. V, dealing with both carrier thermalization and recombination kinetics. The complete analysis of the experimental results based on the model introduced in Sec. V is contained in Sec. VI. The PL data and its connection with our PM data and theory are presented in Sec. VII. Final remarks and conclusions are stated in Sec. VIII.

II. EXPERIMENTAL TECHNIQUE

Transient modulation of the sample's absorption is produced optically using pulsed laser excitation. The ob-

served changes in absorption ($\Delta\alpha$) arise from the redistribution of carriers within the gap states. Absorption increases when the occupancy of initial states is increased or the occupancy of final states is reduced and decreases below the dark level when the occupancy of initial states is reduced or the occupancy of final states is increased. These photoinduced absorption and bleaching signals thus provide information about the distribution of excess carriers trapped in the gap states.[8] Detection of these changes is obtained by monitoring, in real time, the relative change in transmission of a sub-gap cw probe beam. The apparatus used in these experiments (Fig. 1) differs from its predecessors[10,15] in its ability to measure PM decays over many relatively narrow bands of probe wavelengths and in its 10^{-9} minimum detectable $\Delta T/T$. This is 10^3 times better than that previously obtained in the earlier wide-band experiments.

The inherent difficulty in obtaining good signal-to-noise ratios in these measurements arises from the loss of probe beam thoughput. This has been overcome by two approaches. The first is to use pairs of long and short pass interference filters positioned at the probe source rather than using a monochromator located in front of the detector.[15] With this arrangement, the reduction in intensity occurs before the sample allowing the use of higher probe power while maintaining reasonably low sample illumination.[16] In addition, since the filters have a much wider passband than that of a monochromator, less light is lost. The sacrifice in resolution is not important in the case of a-Si:H since this material does not exhibit sharp spectral structure.[9,17]

Twelve pairs of filters are employed providing 12 partially overlapping bands of measurement. Two probe sources and two detectors are needed to cover the entire spectrum from 5.5 to 0.75 μm. For the shorter wavelengths, a tungsten filament in a halogen-filled quartz bulb in conjunction with a germanium detector is used while at longer wavelengths a liquid-nitrogen-cooled InSb detector and Opperman source are employed.

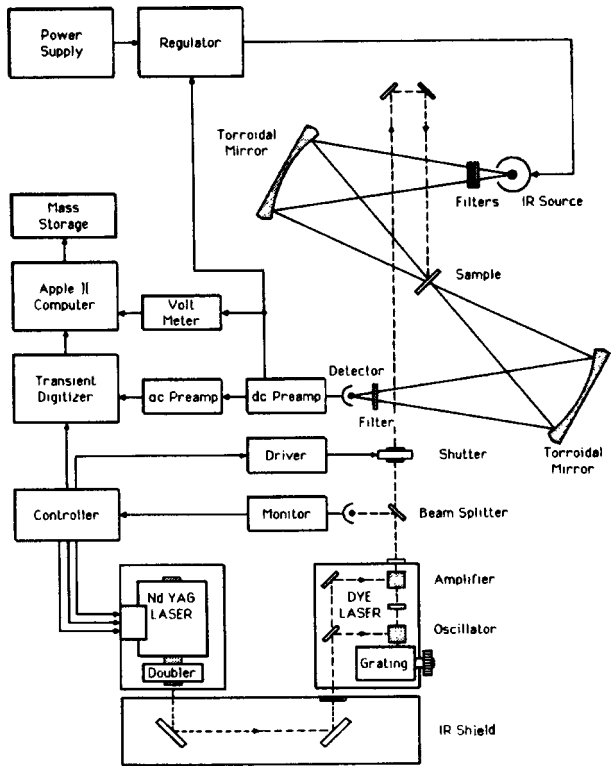

FIG. 1. Block diagram of the experimental apparatus.

The second approach to noise reduction involves the use of several dedicated preamplifier pairs, composed of a dc transconductance amplifier and an ac voltage amplifier. Each dc amplifier is designed to be signal-to-noise ratio optimized for a particular detector. Furthermore, the measurement of transients has been divided into four overlapping time ranges in which each subsequent range has a dwell time which is 20 times larger than that of the previous range. The design of both ac and dc amplifiers is specific to the bandwidth requirements of the time range for which they are intended. Signal transients are averaged over about 10^4 pulses and then transferred to mass storage for later splicing on a logarithmic time scale. Examples of the spliced decays obtained for all 12 energy ranges at a sample temperature of 150 K are given in Fig. 2.

The fluctuations in the Opperman source due to air

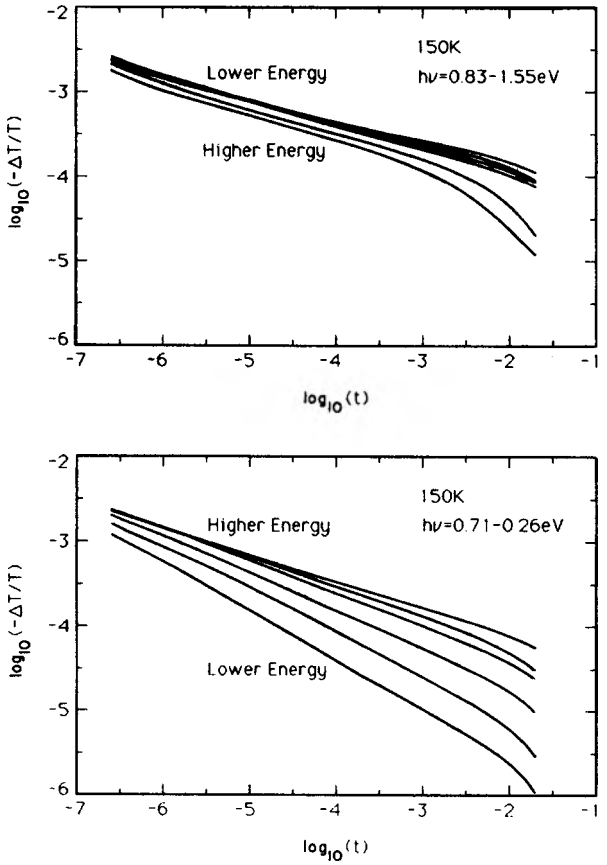

FIG. 2. The upper figure shows the decay of the PM signal on a log-log scale measured at 150 K for six probe energy bands approximately 0.2 eV wide centered on 0.81, 0.87, 1.02, 1.08, 1.30, and 1.55 eV. The curves with the largest amplitude signal correspond to the lowest energies. The lower figure shows the decay of PM measured under the same conditions but using lower probe energy bands of 0.1 eV width centered on 0.71, 0.66, 0.57, 0.46, 0.35, and 0.26 eV. Here, the higher-energy signals have the highest amplitude.

currents limit signal-to-noise ratio at long wavelengths. Long-term drift is reduced actively by sending a control signal derived from the output of the detector's dc amplifier to the regulator while short-term drift is reduced passively by shielding the source.

The pump beam is obtained from a dye laser which is excited by a doubled Q-switched Nd:YAG (YAG denotes yttrium-aluminium-garnet) laser. Final pulse duration is 10 ns with a photon energy of 2.1 eV. The energy per pulse at the sample is 50 $\mu J/cm^2$. The YAG repetition rate of 20 Hz is often too fast to allow for complete carrier relaxation. For this reason, a synchronously operated shutter is placed in the path of the pump beam enabling a selection of repetition rates given by $20/n$ Hz where $n=1,2,\ldots,100$. To synchronize all system events, we have devised the timing circuit labeled controller in Fig. 1. It supplies pretrigger pulses to the digitizers, operates the shutter, and sends oscillator, lamp, and Q-switch triggers to the YAG. The average output power of the dye laser is stabilized by a feedback network which adjusts the delay time between Q-switch and flashlamp trigger events in order to control output intensity according to an internally referenced error signal generated by the monitor.

Depending on the sample and its temperature, a photoluminescence signal at 1.1–1.4 eV (Ref. 18) may accompany the photomodulation signal. This is dealt with by placing additional filters in front of the detector which match the passband of the first set of filters. In addition, an independent measurement of the luminescence is made upon blocking the probe beam. This is then recorded for later subtraction from ΔT. Although a nuisance to photomodulation spectroscopy, transient-photoluminescence spectra do contain valuable additional information and have been studied in detail by others. We have measured PL using our apparatus under the same conditions as the PM measurements so that a direct comparison can be made. This is done by removal of the probe beam and relocation of the filters in front of the detector.

III. EXPERIMENTAL RESULTS

Spectrally resolved transient photomodulation was measured on samples of high-quality (low-defect) undoped a-Si:H produced by Xerox Corporation and Harvard University. The data reported here were obtained from a single 5-μm-thick film from the Harvard group deposited on sapphire by the glow-discharge method. Complete sets of spectrally resolved PM decays were obtained from this sample at temperatures of 10, 80, 150, and 220 K. Examples of the results are shown in Figs. 3 and 4 where we have plotted $-\Delta T/T$ in the form of spectra at fixed time delays for the 10- and 220-K data, respectively. The dependence of $-\Delta T/T$ on temperature at 10 μs after excitation is shown in Fig. 5. Data obtained from the other samples produced similar results.

Three onsets in absorption are observed in these figures corresponding to three distinct sets of excess carriers trapped inside the band gap. The lowest energy onset occurs at 0.15 eV and shifts to higher energy as time and/or temperature increases. The energy of this transition indicates a bandtail to extended state transition.[9]

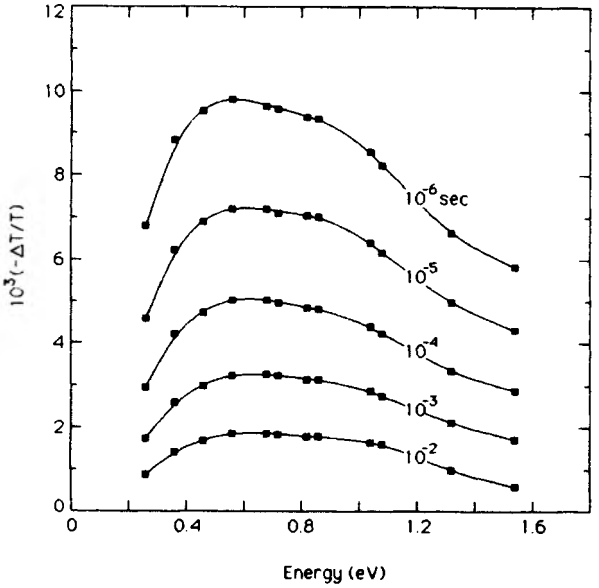

FIG. 3. This is an example of the time evolution of a PM spectrum measured at 10 K. Two positive onsets and one negative onset are present in which the low-energy onset is seen to have the most rapid decay.

According to measurements of ir quenched LESR, transitions involving the valence band dominate.[19] The shift in onset energy with time is due to a combination of thermalization and recombination processes whose rates are strongly temperature dependent. Note from Fig. 5 that at 220 K this signal is completely absent.

The second absorption onset, occurring at about 0.65 eV, is believed to be due to an excess of electrons trapped on negatively charged dangling bond states (D^-) which absorb photons via transition to the conduction band.[20]

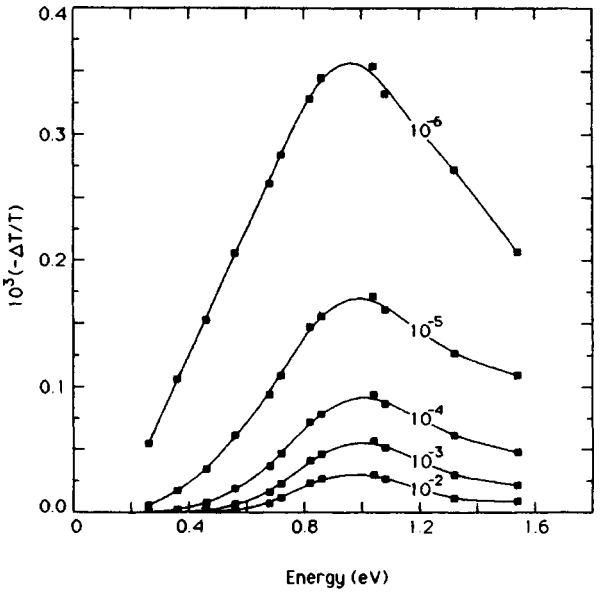

FIG. 4. This set of spectra was measured at 220 K. Note the rapid disappearance of the low-energy band in comparison to the 10-K data of Fig. 3.

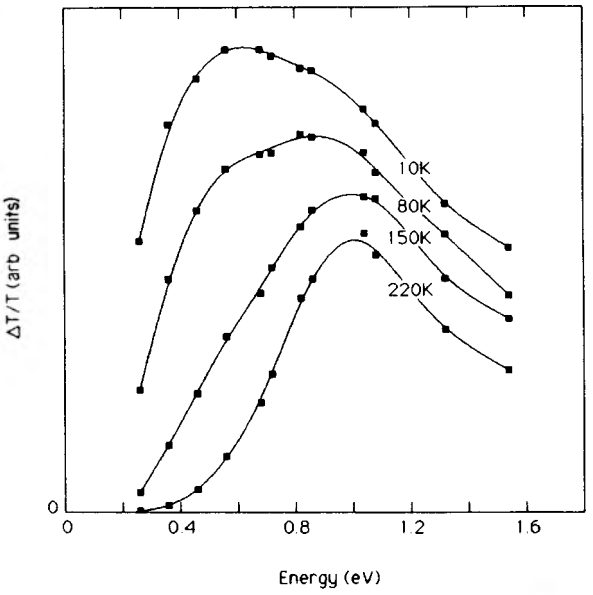

FIG. 5. On this figure are plotted PM spectra at $T=10$, 80, 150, and 220 K measured at the fixed time delay of 10^{-5} s following excitation. A clear separation of the absorptive PM onsets and their strong temperature dependence is observed.

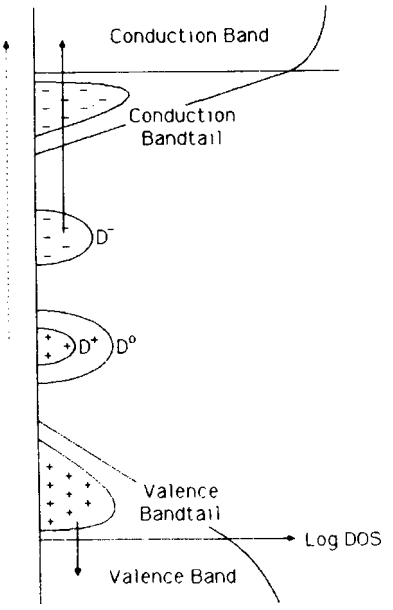

FIG. 6. Diagram of states in the gap in which PM active transitions are shown. The solid lines correspond to the transitions associated with an absorptive photomodulated signal while the dashed line corresponds to the transition which is reduced by excitation resulting in the bleached 1.06-eV signal.

These carriers are probably the same as those responsible for the 0.9-eV defect photoluminescence signal reported by others[1,2,18] involving the radiative transition of an electron from D^- to a valence hole. Both PL and our PM measurements show weak temperature dependences in both the shift and decay of this band. The temperature dependence of the PM decay is sufficiently small compared to that of the trapped holes that, at high temperatures, this band dominates. This is analogous to the fact that the defect PL can only be observed at high temperatures[1] where the bandtail PL signal is small enough so as to not obscure the defect band.

Finally, a negative absorption signal is seen to begin at about 1.08 eV. It is associated with the bleaching of the electron transition which has, as initial and final states, respectively, neutral dangling bond states (D^0) and the conduction band.[21,22] This is consistent with our interpretation of the second onset since an increase in D^- implies a corresponding reduction in D^0.[20] Furthermore, the spread of the carriers in energy as deduced from the onsets is the same for both bands. The 0.43-eV difference between the two onset energies is due to the dangling bond correlation energy.[8,23,24] A detailed comparison of the decay of the defect absorption and bleaching signals shows identical time dependences.[25] Refer to Fig. 6 for a picture of the states in the gap in which the PM active transitions have been illustrated.

IV. DISTRIBUTION OF CARRIERS

It is not possible to determine the actual density of excess carriers trapped in the gap, however, a closely related quantity proportional to the product of the density of excess carriers with the square of the transition matrix element can be computed. This distribution will be referred to as the effective carrier density $\Delta n_{\text{eff}}(E)$. The connection between $\Delta n_{\text{eff}}(E)$ and its PM spectrum at a fixed time is given by the linear relationship[25]

$$(\Delta T/T)_i \propto \int_0^{E_g} dE\, \Delta n_{\text{eff}}(E)\Gamma_i(E)\ , \tag{4.1}$$

where $(\Delta T/T)_i$ is the relative change in transmission measured in the ith energy range. The response functions $\Gamma_i(E)$ are the energy-dependent weight factors to be applied to Δn_{eff} prior to integration over the band gap. Each function takes into account the density of final (extended) states, and the spread of the ith filter's passband. Assuming a square-root DOS for both the conduction and valence bands, $\Gamma_i(E)$ is explicitly given by[25]

$$\Gamma_i(E) \propto \int_E^{\infty} d(h\nu) G_i(h\nu) \frac{(h\nu - E)^{1/2}}{h\nu}\ , \tag{4.2}$$

where G_i is the normalized filter transmission function for the ith energy range.

The problem to be addressed now is the inversion of (4.1) for the distribution of excess carriers. Direct inversion is not possible since $\Delta n_{\text{eff}}(E)$ is nonuniquely determined by the 12 discrete samples $(\Delta T/T)_i$. Constraints are required. The approach we use is to model the distribution of carriers using parametrized functions.[25] The parameters of the model are varied until a best fit is obtained to the set of $(\Delta T/T)_i$. Since three onsets have been discerned from the spectra, we have chosen to use a superposition of three finite-extent functions for our model. Denoting the functional form of the distribution of carriers trapped on D^- and D^0 as $\rho_{\text{DB}}(E)$ and the functional form of the distribution of bandtail holes as

$\rho_{BT}(E)$, the parametrized distribution of carriers is

$$\Delta n_{\text{eff}}(E) = A\rho_{BT}((E-E_d)/E_0) + B\rho_{DB}((E-E_1)/\Delta E) - C\rho_{DP}((E-E_2)/\Delta E) , \quad (4.3)$$

where $\{A,B,C,E_d,E_0,E_1,E_2,\Delta E\}$ constitute the complete set of adjustable parameters. We have chosen $\rho_{DB}(E)$ to be the Gaussian distribution and use for $\rho_{BT}(E)$ a function obtained by numerical methods applied to the theory of thermalization by hopping in exponential bandtails. This will be described in detail in Sec. V.

The formulation of the problem is to find the set of parameters which minimizes the square error,

$$\sigma^2 = \sum_i \left| (\Delta T/T)_i - \int dE\, \Delta n_{\text{eff}}(E)\Gamma_i(E) \right|^2 , \quad (4.4)$$

to the experimental values of $(\Delta T/T)_i$ independently for each point in time and temperature. The numerical technique employed to search the eight-dimensional parameter space for the minimum value of σ^2 is the simplex method. The distribution obtained by this procedure for the 150 K data is shown in Fig. 7.

Taking into account all four temperatures, the fitting parameters E_1 and E_2 place the position of the DB absorption and bleaching signals at about 0.65±0.05 and 1.08±0.04 eV, respectively. Assuming uniform occupancy of the dangling bonds, the width of these states is 0.26±0.03 eV full width at half maximum (FWHM).

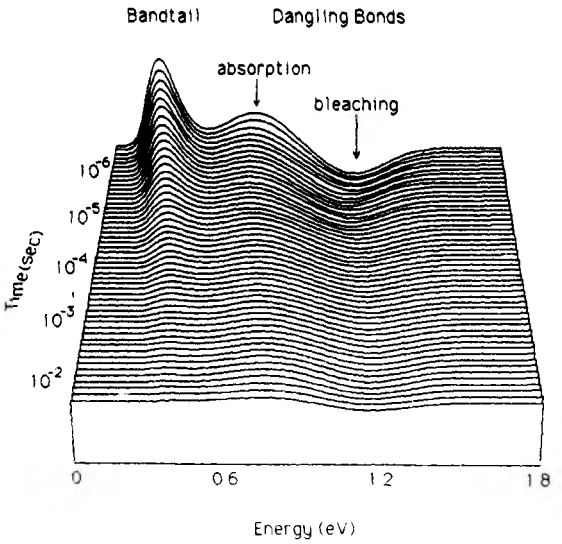

FIG. 7. Three-dimensional representation of the distribution of trapped carriers as a function of logarithmic time (increasing out of page) and probe energy (increasing to the right) reconstructed from the 150-K data.

V. THEORY OF CARRIER KINETICS

A. Introduction

In this section we obtain analytical expressions which describe the time dependent distribution of excess carriers in an exponential bandtail following pulsed excitation. This work has been motivated by the lack of such expressions in the literature although a great deal of theoretical and computational attention has been given to the problem.[11–14,26] Many approximations have been made in order to achieve our results, the choice of which, and their justification, is based on the condition that agreement with the data be maintained.

B. Thermalization

We begin by considering the thermalization of nonequilibrated carriers in a system of localized states. The starting point for this treatment is the linearized master equation[27]

$$dq_i(t)/dt = -q_i(t)\sum_j w_{ij} + \sum_j w_{ji}q_j(t) , \quad (5.1)$$

where $q_i(t)$ is the probability that state i is occupied at time t and w_{ij} is the pair transition rate between an initial state i and a final state j. The neglect of the second-order terms which appear in the general master equation assumes that the average occupancy of states is small. (This is justified later.) The integral form of this equation is[25]

$$q_i(t) = q_i(0)s_i(t) + \sum_j w_{ji}\int_0^t dt' q_j(t')s_i(t-t') , \quad (5.2)$$

where $s_i(t)$, given by

$$s_i(t) = \exp\left[-\sum_j w_{ij}t\right] , \quad (5.3)$$

is the probability that a carrier survives in state i for a time interval t.

The dependence of the survival probability $s_i(t)$ on the energy of the site is of particular importance to the remaining discussions of this section. We will evaluate (5.3) in a statistical sense by integrating over all possible positions and energies of the final states j weighted by the probability $P(\mathbf{r}_1,\ldots,\mathbf{r}_N;E_1,\ldots,E_N)$ of their occurrence. This process will incorporate into the survival probability associated with a state all that is known of its surroundings. Symbolically, the operation of configuration averaging is expressed as

$$\langle\ \rangle_{\{j\}} = \int d^3r_1 \cdots \int d^3r_N \int dE_1 \cdots \int dE_N P(\mathbf{r}_1,..,\mathbf{r}_N;E_1,\ldots,E_N) , \quad (5.4)$$

where each subscript corresponds to a particular state of the subsystem. Since we will be dealing with distributions which are spatially homogeneous, the configuration averaged $s_i(t)$ can only depend on the state's energy and not its position. Dropping the subscript i in favor of the continuous variable E, the definition of the survival probability $S(E,t)$ in the continuum limit is

$$S(E,t)=\left\langle \exp\left[-\sum W(r_j,E-E_j)t\right]\right\rangle_{\{j\}}, \tag{5.5}$$

where w_{ij} has been replaced by its continuum equivalent $W(r_j,E-E_j)$ and r_j is the distance to site j. Due to a lack of correlation between the arrangement of states, P can be factored into the product of N identical probability distributions as

$$P(\mathbf{r}_1,\ldots,\mathbf{r}_N;E_1,\ldots,E_N) = p(r_1,E_1)p(r_2,E_2)\cdots p(r_N,E_N) . \tag{5.6}$$

This decouples the N sets of integrals into the product of N equal factors expressed by

$$S(E,t)=\left[\int d^3r\int dE' p(\mathbf{r},E')e^{-W(r,E-E')t}\right]^N, \tag{5.7}$$

which displays the nature of S as arising from the probability a carrier survives transition to N independent and equally distributed parallel channels.

In order to evaluate (5.7) it is necessary to take the limit as $N\to\infty$ and let the volume over which the space integral is performed to become infinite in order to keep the density of states $n_0=N/V$ finite. To utilize this limit, note that the time derivative of (5.7),

$$dS(E,t)/dt=-S^{(N-1)/N}(E,t)\times\int d^3r\int dE'\,Np(\mathbf{r},E')\times W(r,E-E')e^{-W(r,E-E')t} , \tag{5.8}$$

contains a power of $S(E,t)$ which becomes unity as $N\to\infty$. Upon replacing $Np(\mathbf{r},E')$ by the volume-energy density of states $G(\mathbf{r},E')$ one arrives at

$$d\ln S(E,t)/dt=-\int d^3r\int dE' G(\mathbf{r},E')\times W(r,E-E')e^{-W(r,E-E')t} , \tag{5.9}$$

which can immediately be integrated back over time to obtain

$$\ln S(E,t)=-\int d^3r\int dE' G(\mathbf{r},E')\times(1-e^{-W(r,E-E')t}) . \tag{5.10}$$

This is a generalization of a result originally obtained by Thomas *et al.*, in conjunction with tunneling transitions between randomly distributed donor-acceptor pairs.[28]

The pair rate function $W(r,\Delta E)$ appearing in (5.10) is assumed by most authors[13,14,26] to have the following exponential dependence on distance and energy separation:

$$W(r,\Delta E)=\nu_0 e^{-2r/a}e^{-\Theta(\Delta E)\Delta E/kT} . \tag{5.11}$$

The unit step function $\Theta(\Delta E)$ restricts the energy dependence to upward ($\uparrow$) transitions only. Thus, downward ($\downarrow$) transitions go at a rate which is independent of the energy lost whereas $\uparrow$ transitions are slowed down by the need to acquire energy from the lattice. The parameter a corresponds to the localization length of the larger wave function involved in the transition. The prefactor ν_0 contains all the other factors which determine the fundamental rate of the transitions. For radiative transitions, the value of 10^8 Hz is typical,[18] and for nonradiative transitions, values between 10^{12} and 10^{13} Hz are favored.[3,11]

C. Thermalization in exponential bandtails

The appropriate density of states for an exponential bandtail is one which is spatially isotropic and exponentially decreasing into the gap. Thus we have

$$G(\mathbf{r},E)=(n_0/E_0)e^{-E/E_0}=n_0 g(E) , \tag{5.12}$$

where E_0 is the width of the tail, n_0 is its total density of states, and $g(E)$ specifies the exponential shape of the tail. The energy scale used here is positive in the gap and zero at the mobility edge.

Analytic evaluation of the integrals in (5.10) require only that the functional form $\exp(-e^{-z})$ can be approximated by $\Theta(z)(1-e^{-z})$. During the course of the evaluation it becomes natural to introduce the logarithmic time parameter $x=\ln(\nu_0 t)$ and the dispersion parameter $\alpha=kT/E_0$. In terms of these new parameters, the result of the calculation gives

$$\ln S(E,x)=-N_{\rm bt}e^{-E/E_0}F(x) , \tag{5.13}$$

where $N_{\rm bt}=n_0\pi a^3$ is a measure of the number of states per wave-function volume and the combined factor $N_{\rm bt}e^{-E/E_0}$ is the number of states per wave-function volume which are energetically below E.

The time dependence, governed by the function $F(x)$, is comprised of two contributions. The first, $F^{\downarrow}(x)$, involves only $\downarrow$ transitions, and the second $F^{\uparrow}(x)$ involves only $\uparrow$ transitions. Explicitly, these are[25]

$$F^{\downarrow}(x)=\begin{cases} e^x, & x<0 \\ 1+x+x^2/2+x^3/6, & x>0 \end{cases} \tag{5.14}$$

and

$$F^{\uparrow}(x)=\begin{cases} \alpha e^x/(1-\alpha), & x>0 \\ Ae^{\alpha x}-B_0-B_1\alpha x-B_2(\alpha x)^2/2-B_3(\alpha x)^3/6, & x<0 \end{cases} \tag{5.15}$$

where

$$A=1/(1-\alpha)+1+1/\alpha+2/\alpha^2+1/\alpha^3 ,$$

$$B_0=1+1/\alpha+2/\alpha^2+1/\alpha^3 ,$$

$$B_1=1/\alpha+2/\alpha^2+1/\alpha^3 ,$$

$$B_2=2/\alpha^2+1/\alpha^3 ,$$

$$B_3=1/\alpha^3 .$$

The total $F(x)$ is obtained by summing the above two contributions together;

$$F(x)=F^{\downarrow}(x)+F^{\uparrow}(x) . \tag{5.16}$$

It can be verified that as $T\rightarrow 0$, $F(x)\rightarrow F^{\downarrow}(x)$.

An interesting behavior of the survival probability is brought out by noting that according to (5.13) the dependence of S on E and x involves the product of a function of E and a function of x only. This allows $S(E,x)$ to be cast into the form

$$S(E,x)=\exp(-e^{-[E-E_d(x)]/E_0})\approx\Theta(E-E_d(x)) , \tag{5.17}$$

where $E_d(x)=E_0\ln[N_{bt}F(x)]$. Physically, E_d is a demarcation line between those states which have already released their carriers and those which have not yet done so just as it is in the multiple trapping model.[11,12] As time progresses, E_d monotonically shifts into the gap. Figure 8 shows curves of E_d versus x for various α. At long times, two simple limiting forms of $E_d(x)$ emerge for small[13] and large[11] α. These are

$$E_d(x)=E_d\ln(N_{bt}/6)+3E_0\ln(x) \quad \text{for } \alpha=0 , \tag{5.18}$$

and

$$E_d(x)=E_0\ln(AN_{bt})+kTx \quad \text{for } \alpha>\tfrac{1}{2} . \tag{5.19}$$

The first involves ↓ transitions whereas the second involves only ↑ transitions.

An important question to consider is how the releases are divided between ↑ and ↓ transitions. It turns out that prior to a particular time x_s (similar but not the same as the segregation time t_s defined by Monroe[13]), carriers prefer ↓ transitions over ↑ ones. After x_s, the reverse situation is true. To illustrate this mathematically, we need to first introduce the conditional transition rates $R^{\uparrow}(E,x)$ and $R^{\downarrow}(E,x)$ corresponding to the ↑ and ↓ rates for a carrier leaving a state at energy E given that it has already survived for a time x. The probability the carrier survives against an ↑ transition for a time x and then undergoes an ↑ transition in the interval dx is just $-dS^{\uparrow}$. Inclusion of the probability it survives any transition is obtained by multiplying this with the probability $S^{\downarrow}$ that it also survives against a ↓ transition. Upon normalizing this result to the total survival probability $S=S^{\uparrow}S^{\downarrow}$ we arrive at

$$R^{\uparrow}(E,x)=\frac{d\ln S^{\uparrow}(E,x)}{dx} \text{ and } R^{\downarrow}(E,x)=-\frac{d\ln S^{\downarrow}(E,x)}{dx} . \tag{5.20}$$

Of course, the net conditional transition rate, obtained by adding the above rates, as required gives

$$R(E,x)=\frac{d[\ln S^{\uparrow}(E,x)+\ln S^{\downarrow}(E,x)]}{dx} =-\frac{d\ln[S^{\uparrow}(E,x)S^{\downarrow}(E,x)]}{dx}=-\frac{d\ln S(E,x)}{dx} . \tag{5.21}$$

Upon setting the individual rates of (5.20) equal to each other, the transcendental equation

$$dF^{\uparrow}(x)/dx=dF^{\downarrow}x/dx$$

is obtained whose root defines the segregation time x_s. The numerical solution is plotted in Fig. 9. In the region

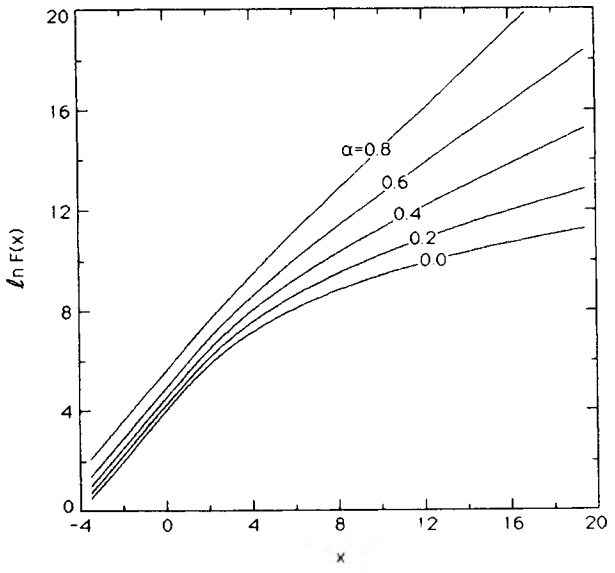

FIG. 8. Theoretically predicted shift in demarcation energy as a function of $x=\ln(\nu_0 t)$ for various values of $\alpha=kT/E_0$.

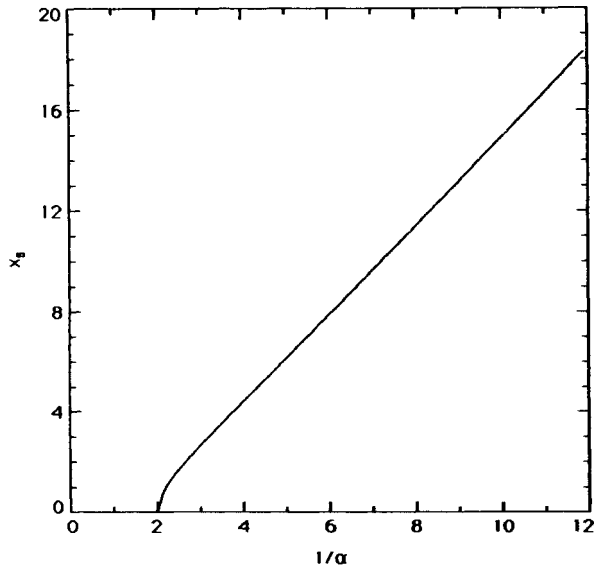

FIG. 9. Theoretically predicted segregation time plotted as $x_s=\ln(\nu_0 t_s)$ vs $1/\alpha=E_0/kT$ defined as the time in which the upward and downward release rates are equal.

of $\alpha > \frac{1}{2}$, $\uparrow$ transitions always dominate (i.e., $t_s = 0$). This result is obvious when one considers that for $\alpha = \frac{1}{2}$ the number of available higher energy states, determined by the product of the rate factor $e^{-\Delta E/kT}$ with the exponentially increasing DOS, exactly matches the available DOS of lower states. This leads to the important conclusion that *for $T > T_0/2$ the standard treatment of MT (Refs. 11, 12, and 26) involving the extended states above the mobility edge must be used.*

D. Recombination

Recombination can occur by direct tunneling of an electron in the conduction-band tail to a trapped hole in the valence-band tail or may proceed via an intermediate state located deep in the gap in which either the electron will trap first followed by hole capture or vice versa.[18] According to Shockley-Read theory the latter recombination process is monomolecular with a time dependence which is governed by the slower of the two capture rates.[29] As will be seen in the next section, the data indicate a monomolecular process rather than a bimolecular one over the range of experimental times and excitation intensities. Bimolecular recombination is indicated at shorter times due to the nonlinear dependence of the carrier density on excitation intensity measured at the earliest time,[25,30] although as will be pointed out later, dispersion can also account for this effect.

Inclusion of a monomolecular recombination mechanism is formally achieved by appending onto the master equation (5.1) an additional term which contains the transition rate to recombination centers. In the monomolecular case, this produces

$$\frac{dq_i(t)}{dt} = \sum_j w_{ji} q_j(t) - q_i(t) \left[\sum_j w_{ij} + \sum_k w'_{ik} \right] , \tag{5.22}$$

where k indexes recombination centers. The additional number of possible transitions provided by recombination will decrease the overall survival probability of the carriers against release by a multiplicative factor S' equal to the survival probability against direct recombination. This is in analogy to the rule $S = S^{\uparrow} S^{\downarrow}$.

Since the recombination centers, like the bandtail states, are randomly distributed in space, the results obtained in the calculation of S are applicable to S'. In this case, however, only $F^{\downarrow}(x)$ contributes since all recombination transitions are downwards in energy. Likewise, the number of recombination centers below any given bandtail state is independent of the state's energy. From these considerations, one obtains the energy independent recombination probability through

$$\ln S'(x) = -N_{\rm rc} F^{\downarrow}(x) , \tag{5.23}$$

where $N_{\rm rc}$ is the number of recombination centers contained within the volume of the larger wave function of the two states involved. The total survival probability $S_{\rm T}$ against both intrabandtail and recombination transitions is then

$$S_{\rm T}(E,x) = S(E,x) S'(x) . \tag{5.24}$$

It is apparent from this relation that the survival probability is reduced uniformly in energy. This in turn leads to the important conclusion that *the demarcation energy is not affected by recombination.* The origin of this result traces back to the linear form we have assumed for the master equation in which saturation effects are ignored.

We begin now the calculation of the decay of the total carrier population due to losses by recombination. From the point of view of a recombination center k, the rate at which carriers are arriving from the bandtail is

$$dq_k(t)/dt = \sum_i q_i(t) w'_{ik} . \tag{5.25}$$

A new quantity $r_i(t)$, defined as the negative change in $q_i(t)$ due to bandtail departures only, is given by the second term in (5.22) as

$$r_i(t) = q_i(t) \left[\sum_j w_{ij} + \sum_k w'_{ik} \right] . \tag{5.26}$$

Using this as a definition of $q_i(t)$, the expression for the total recombination rate obtained by summing (5.25) over all recombination centers k takes the form

$$dN(t)/dt = \sum_i \eta_i r_i(t) , \tag{5.27}$$

where, by conservation of carriers, $-N(t)$ may be interpreted as the total number of carriers remaining in the bandtail at time t and

$$\eta_i = \frac{\sum_k w'_{ik}}{\sum_j w_{ij} + \sum_k w'_{ik}} \tag{5.28}$$

is the efficiency of recombination relative to all other transitions.

The next step is to configuration average η around an arbitrary energy E. Because correlations between the numerator and denominator may be important it is not sufficient to average them separately. The trick to dealing with this problem is to reexpress (5.28) as

$$\eta_i = -\int dt \, \exp\left[-t \sum_j w_{ij} \right] \sum_k w'_{ik} \exp\left[-t \sum_k w'_{ik} \right] , \tag{5.29}$$

and then configuration average over the j and k states independently. This results in the energy-dependent recombination efficiency

$$\eta(E) = -\int dS' S(E,x) . \tag{5.30}$$

The appropriate form of $S(E,x)$ to use, for reasons which will be obvious later, is that for $\downarrow$ transitions only. Upon integration of (5.30), one obtains exactly

$$\eta(E) = \frac{N_{\rm rc}}{N_{\rm rc} + N_{\rm bt} e^{-E/E_0}} , \tag{5.31}$$

which has the intuitive meaning that the probability a carrier at an energy E makes a transition to a recombination center, rather than retrapping at a lower energy, is just the ratio of the effective density of recombination

sites to the total effective density of all sites below E.

By taking (5.27) to the continuum and infinite volume limit, the integro-differential equation

$$dn(x)/dx = -\int dE\, \eta(E) n(E,x) R(E,x) , \tag{5.32}$$

relating the total carrier density $n(x)$ to the carrier density distribution $n(E,x)$, is obtained where $R(E,x)$, as the continuum version of $r_i(t)$, specifies the distribution of release rates per carrier. The physical interpretation of (5.32) is that the number of carriers lost between x and $x+dx$ is given by the product of the number of carriers released in this interval multiplied by the fraction which recombine, integrated over all energy. The release rate $R(E,x)$ has already been defined in terms of S by (5.21). Substitution of S_T for S into this definition gives

$$R(E,x) = -\frac{d}{dx}\ln S(E,x) - \frac{d}{dx}\ln S'(x) . \tag{5.33}$$

The first term involves only those carriers residing near E_d while the second term is uniformly contributed to by all carriers.

In order to solve (5.32) for $n(x)$ it is necessary to make some assumption about the distribution of $n(E,x)$. The simplest way to do this is to remember that

$$S(E,x) \approx \Theta(E - E_d(x)) . \tag{5.34}$$

Taking this to be exactly true implies that the density of carriers has to be given by

$$n(E,x) = n(x) g(E - E_d(x)) \Theta(E - E_d(x)) , \tag{5.35}$$

corresponding to a uniformly occupied bandtail up to the demarcation energy. Note that $n(E,x)$ is properly normalized in the sense that $\int dE\, n(E,x) = n(x)$. Substitution of (5.34) and (5.23) into (5.33) gives

$$R(E,x) = \delta(E - E_d(x)) \frac{d}{dx}(E_d/E_0) + N_{rc}\frac{dF^{\downarrow}(x)}{dx} , \tag{5.36}$$

where the first term corresponds to the releases at the demarcation energy due to bandtail thermalization and the second term gives the energy-independent release rate introduced by the presence of recombination centers. Note that it is not correct to assume that releases of the first type end up retrapping and those of the second type recombine. There is always the possibility that a recombination center lies closer than the nearest trap and vice versa. This is exactly what $\eta(E)$ takes into account. Furthermore, a carrier which is released upwards from E_d may very well execute multiple hops before it is either retrapped below E_d or undergoes recombination. Still, given that its inevitable outcome is one or the other, the efficiency remains the same.

As a first approximation, valid for the case of a low recombination center effective density, we will ignore the second term of (5.36). In this situation of releases from the demarcation energy only, (5.32) in conjunction with (5.35) gives

$$\frac{d}{dx}\ln(n) = -\eta(E_d)\frac{d}{dx}(E_d/E_0) . \tag{5.37}$$

Using the definition of $\eta(E)$ in (5.31), a separable differential equation is obtained which integrates easily with respect to e^{E_d/E_0} giving

$$Q(x) = [1 + (N_{rc}/N_{bt}) e^{E_d(x)/E_0}]^{-1} , \tag{5.38}$$

where $Q(x) = n(x)/n(-\infty)$ is the fraction of the number of initial carriers remaining, alternately interpreted as the survival probability against recombination. Thus the time dependence of the decay is completely specified by the already known function $E_d(x)$. In Fig. 10, graphs of $\ln Q$ versus x are plotted for various α. According to (5.18) and (5.19), this has the low- and high-temperature limiting forms valid for $t \gg 1/\nu_0$ given by

$$Q(t) = [1 - (N_{rc}/6)\ln^3(\nu_0 t)]^{-1} \tag{5.39}$$

and

$$Q(t) = [1 + (t/t_0)^{\alpha}]^{-1} \quad \text{where } t_0 = \nu_0^{-1}(AN_{rc})^{-1/\alpha} . \tag{5.40}$$

The similarity of these expressions to those obtained from energy-independent hopping[31] and multiple trapping[11,12] imply that *this is a general model which contains as temperature limits both hopping and multiple trapping features.*

E. Recombination by direct tunneling

We will now consider how these results are modified by the inclusion of the direct release bandtail carriers to a fixed number of recombination centers. Since (5.32) implies that $\ln Q$ is linear in R, the general expression for $\ln Q$ is composed of the sum of two contributions which we will write as $\ln Q_T = \ln Q + \ln Q'$, where $\ln Q$ is as previ-

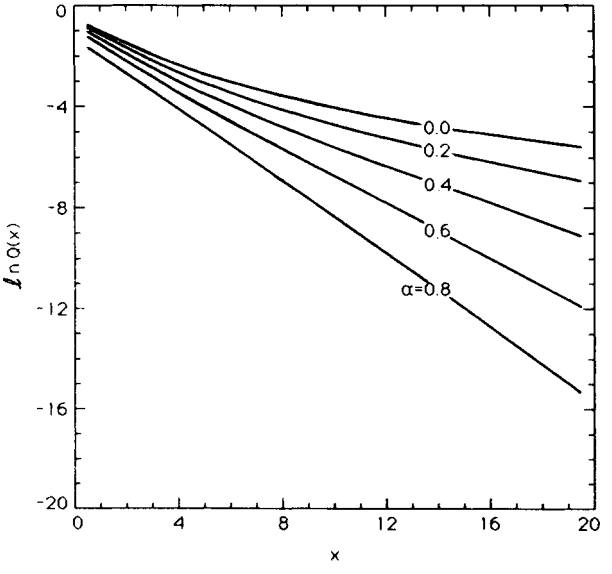

FIG. 10. Log-log plot of the total probability a carrier does not recombine as a result of an upward release vs time in the case of monomolecular recombination for various α where $\alpha = kT/E_0$.

ously defined and $\ln Q'$ contains the contribution of the additional releases. Thus we have the general result that

$$Q_T(X)=Q(x)Q'(x)\ , \tag{5.41}$$

with the meaning that the probability a carrier survives against recombination is given by the probability it does not recombine by release at E_d and does not undergo a direct recombination.

The calculation of $\ln Q'$ as prescribed by (5.32) is straight forward. Upon performing the integration over energy and rewriting the differential in x as one in $F^{\downarrow}$, one obtains

$$\ln Q'=-N_{\rm rc}\int dF^{\downarrow}\,\Phi\ln(1+1/\Phi)\ , \tag{5.42}$$

where $\Phi=(N_{\rm rc}/N_{\rm bt})e^{E_d(x)/E_0}$. At long times ($\Phi\gg 1$) the integrand becomes unity so that the integral itself becomes simply $F^{\downarrow}(x)+\text{const}$. The total long-time decay then has the form of

$$Q_T(x)=Q(x)Q'(x)\propto Q(x)e^{-N_{\rm rc}F^{\downarrow}(x)}\ , \tag{5.43}$$

valid for $E_d\gg E_0\ln(N_{\rm bt}/N_{\rm rc})$ as implied by $\Phi\gg 1$. Figure 11 shows graphs of $\ln Q'$ versus x for various $N_{\rm rc}$. In terms of real time this becomes

$$Q_T(t)\propto Q(t)(\nu_0 t)^{-\alpha(t)}\ , \tag{5.44}$$

where

$$\alpha(t)=N_{\rm rc}\left[\frac{1}{\ln(\nu_0 t)}+1+\frac{\ln(\nu_0 t)}{2}+\frac{\ln^2(\nu_0 t)}{6}\right]\ , \tag{5.45}$$

in which $Q'(t)$ has the form of a power-law decay whose exponent increases slowly with time. The fastest decay we had before, as specified by (5.40), behaves like $t^{-\alpha}$

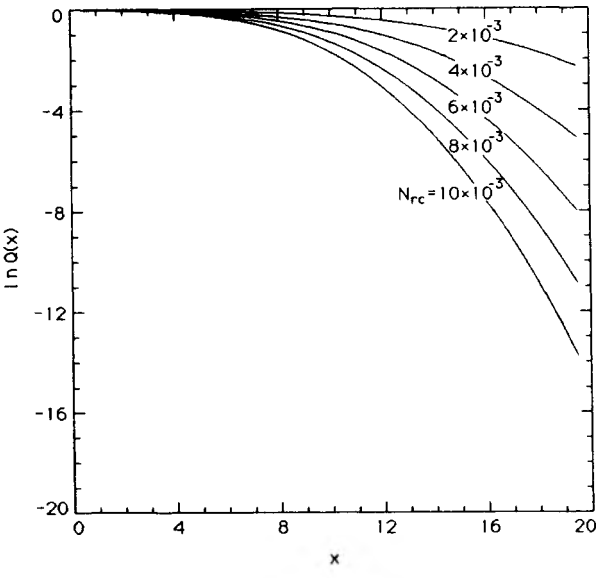

FIG. 11. Log-log plot of the total probability a carrier does not recombine by direct tunneling vs time for various $\alpha=kT/E_0$.

where α is constant. This means that at sufficiently long times, all decays will be governed by the time dependence of Q'. Thus we arrive to the conclusion that *in the monomolecular case, recombination by direct tunneling dominates at long times.*

F. Bimolecular recombination

The time dependence of carrier decay in the situation where bimolecular recombination kinetics holds will now be discussed. Unlike the monomolecular case, the number of recombination centers is not constant in time. One must use the nonlinear master equation

$$d\overline{n}_i/dt=\sum_j w_{ji}\overline{n_j(1-n_i)}-\sum_j w_{ij}\overline{n_i(1-n_j)}-\sum_k w_{ik}\overline{n_i(1-n_k)}\ , \tag{5.46}$$

where $n_i=1$ or 0 depending on whether state i is occupied or not. The average of n_i over an ensemble of identical systems with similar conditions, $\overline{n}_i=q(t)$, is the probability of finding a carrier in i at t. Terms like $\overline{n_i(1-n_j)}$ give the joint probability that i is occupied and j is empty at t. Thus the factor $\overline{n_i(1-n_k)}$ appearing in the recombination part of the master equation corresponds to the joint probability that state i is occupied by an electron and state k is occupied by a hole. Since the number of electrons and holes are taken as equal, the recombination rate is always second order in carrier density. This is the definition of bimolecular kinetics.[10]

We will begin by ignoring possible statistical correlations in $\overline{n_i(1-n_k)}$ so that the simpler form $q_i(t)q_k(t)$ may be used where $q_k(t)$ is to be interpreted as the probability with which state k is not occupied. When this is carried through in the analysis of recombination due to carrier release from the demarcation level only, it is found that the efficiency function η must be modified to the time-dependent form

$$\eta(E,x)=\frac{n(x)}{n(x)+\gamma n_0 e^{-E/E_0}}\ , \tag{5.47}$$

where γ is the ratio of the effective wave-function volumes for tail-tail transitions to that for recombination centers and, as such, is a measure of the relative strength of the two.[25] The difference between (5.47) and the monomolecular version (5.31) is that as time progresses, the recombination efficiency is reduced due to the disappearance of recombination centers.

Paralleling the treatment of the monomolecular case results in the nonlinear rate equation[25]

$$\frac{dn}{dx}=-\frac{n^2(x)}{n(x)+\gamma n_0 e^{-E_d/E_0}}\frac{d}{dx}(E_d/E_0)\ . \tag{5.48}$$

The substitution $\Phi(x)=[n(-\infty)/\gamma n_0]e^{E_d(x)/E_0}$ for the independent variable x and $Q=n/n(-\infty)$ for the dependent variable n results in the simpler differential equation

$$dQ/Q+(\Phi\,dQ+Q\,d\Phi)=0\ , \tag{5.49}$$

which is exact if the independent variable is taken to be $Q\Phi$. The solution for Q in terms of $Q\Phi$, is given by

$$\ln Q + Q\Phi = 0 , \tag{5.50}$$

which is transcendental with respect to Q and Φ independently. Figure 12 contains graphs of $\ln Q$ versus x for various α obtained by numerical solution of (5.50).

The case of bimolecular recombination by direct tunneling has already been treated by the distant pair model (DPM).[31] In the language of this section, the problem DPM solved is equivalent to the solution of (5.46) with the intraband transitions removed:

$$dn_i/dt = -\sum_k w'_{ik} \overline{n_i(1-n_k)} . \tag{5.51}$$

Since each transition corresponds to a recombination, as many carriers are lost from the k states as are lost from the i states. The lack of intraband transitions means that carriers cannot diffuse. At first nearest neighbors recombine, but as time progresses and the number of carriers becomes fewer, the average separation between carriers increases thus slowing down the rate of recombination. The usual averaging process applied to (5.51) yields the continuum equation for $Q(x)$,

$$dQ = -NQ^2 dF^{\downarrow} , \tag{5.52}$$

where N is the initial number of carriers per localization volume. The appearance of Q^2 in determining the rate reflects the bimolecular nature of the process. The solution of (5.52) is

$$Q(x) = [1 + NF^{\downarrow}(x)]^{-1} , \tag{5.53}$$

which, by coincidence, has the same time dependence as recombination by release from E_d at $T=0$. Equation (5.53) is more precise than Dunstan's solution[31] in that it is valid at short times as well as long times. It is also possible to solve (5.51) under the conditions of complete redistribution. In this case, (5.51) is averaged first and then solved giving the nondispersive solution

$$Q(t) = [1 + N(\nu_0 t)]^{-1} . \tag{5.54}$$

In general, the actual decay will take on an intermediate behavior progressing to pure dispersive behavior as the carriers settle in the tails. The contribution to the overall decay due to direct tunneling in the bimolecular regime is then a time dependence which slows with time in the sense that a log-log plot of $Q(x)$ versus x will have positive curvature. Contrast this behavior to the negative curvature decays of the monomolecular case. In conclusion, *the characteristic which identifies the reaction type for recombination by direct tunneling is the sign of the curvature of the decay as seen on a log-log plot of Q versus t.*

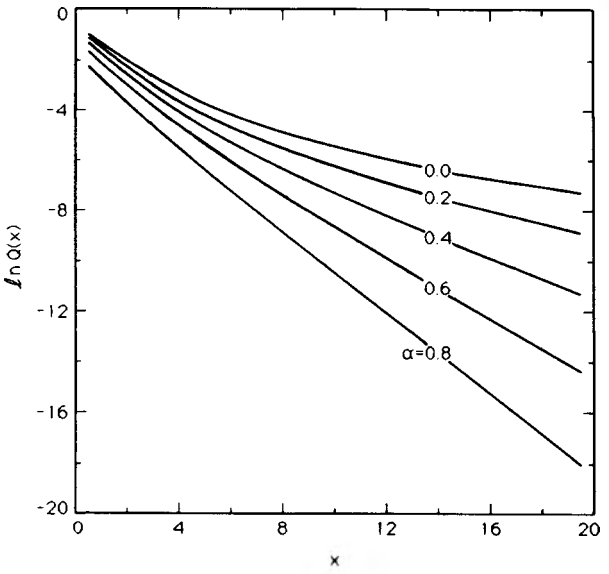

FIG. 12. Log-log plot of the total probability a carrier does not recombine as a result of an upward release vs time in the case of bimolecular recombination for various $\alpha = kT/E_0$.

G. Distribution of carriers

The nonequilibrium distribution of carriers in the bandtail is determined in detail from Eq. (5.2), which gives the probability of finding a carrier on site i at time t. in the continuum and infinite volume limit this becomes

$$\begin{aligned} Q(E,t) = {} & Q(E,0)S(E,t) \\ & + N_{\rm bt} g(E) \int dt' S(E,t-t') \\ & \times \int dE' Q(E',t') \\ & \times W(E-E',t-t') , \end{aligned} \tag{5.55}$$

where as before, $g(E)$ is the normalized exponential DOS, $N_{\rm bt}$ is the number of bandtail states per localization volume, and $S(E,t)$ is given by (5.5). As can be verified by substitution of (5.3) into (5.2) for $s_i(t)$, the definition of $W(E,t)$ is

$$W(E,t) = \langle w_{ji} e^{-w_{ij} t} \rangle . \tag{5.56}$$

The term inside the angular brackets gives the rate at which a carrier trapped on j makes a transition to i and does not return to j in the time interval t. Performing the configuration average over a spatially random distribution of states j of energy E gives

$$W(E,x) = \begin{cases} \nu_0 e^{E/kT} e^{-x} [1 + (x - E/kT) + (x - E/kT)^2], & E > 0 \text{ and } x > E/kT \\ \nu_0, & E > 0 \text{ and } x \le E/kT \\ \nu_0 e^{E/kT} e^{-x} (1 + x + x^2/2), & E < 0 \text{ and } x > 0 \\ \nu_0 e^{E/kT}, & E < 0 \text{ and } x \le 0 \end{cases} \tag{5.57}$$

where again we have used the logarithmic time variable $x = \ln(\nu_0 t)$.

The integral equation (5.55) is solved for $Q(E,t)$ numerically by successive approximation assuming an initial distribution of trapped carriers $Q(E,0)$ which follows the shape $g(E)$ of the exponential DOS. The actual value of the tail width E_0 need not be known at this point since it only appears as E/E_0. We found that, at times long enough for the transient term to decay, a time-independent shape is obtained whose position in energy shifts with the demarcation energy calculated earlier. This asymptotic distribution is the function $\rho_{bt}((E-E_d)/E_0)$ used in Sec. IV. Examples of this distribution are given in Fig. 13. A reasonably good analytical approximation to this distribution is $\rho_{bt}(u)=\frac{2}{3}e^{-2u/3}\exp(-e^{-2u/3})$. This has the same form as that arrived at by Dunstan and Boulitrop[32] but with a width which is greater by a factor of $\frac{3}{2}$.

VI. COMPARISON OF THEORY AND EXPERIMENT

A. Introduction

According to the results of Sec. V, the distribution of bandtail carriers in energy, time, and temperature is completely specified by the three parameters E_0, N_{bt}, and N_{rc}. To determine these constants, the data is refitted using (5.38), (5.43), and (5.14)–(5.16) to provide the time and temperature dependence of the total bandtail decay while the shape of the distribution of carriers in energy is given by ρ_{bt} as previously calculated with $[E-E_d(t,T)]/E_0$ as its argument. Here, $E_d(t,T)$ is the computed demarcation energy given by (5.14)–(5.16) which depends only on N_{bt} and E_0. The procedure then is to find the values of these three quantities which best fit all the data in the sense that

$$\sigma^2=\sum_T\sum_x\sum_i\left[(\Delta T/T)_i-\int dE\,\Delta n_{\rm eff}(E,E_0,N_{bt},N_{rc})\times\Gamma_i(E)\right]^2 \tag{6.1}$$

is minimized where the sums are over *all points in energy, time, and temperature.* The scaling heights of ρ_{bt} are allowed to vary with temperature but not time, and all parameters associated with the DB signals are completely free to vary. Equation (6.1) differs from (4.4) in that the number of fitting parameters associated with the bandtail has been reduced from sets of three for each point in time and temperature to only three for all times and temperatures.

The optimal values of the constants obtained by the three parameter fits are $N_{bt}=4.9\times10^{-2}$, $E_0=46$ meV, and $N_{rc}=1.8\times10^{-4}$ producing a relative σ of about 2%. Taking the localization radius of the valence tail states to be $a=6$ Å,[33] the total tail state density, given by $N_{bt}/(\pi a^3)$, is $n_0=7.2\times10^{19}$ cm^{-3}. This agrees well with the value 6×10^{19} cm^{-3} observed directly by photoemission yield spectroscopy.[34] The tail width of 46 meV is also in close agreement with that of Greip and Ley.[35] Roxlo *et al.*[36] report a value of 48 meV. Discussion of N_{rc} will be deferred until the recombination centers have been identified.

B. Bandtail carriers

A comparison between the total number of observed bandtail carriers obtained from the area under the low-energy bands, such as in Fig. 7, to the theoretical distribution shows excellent agreement. (See Fig. 14.) The

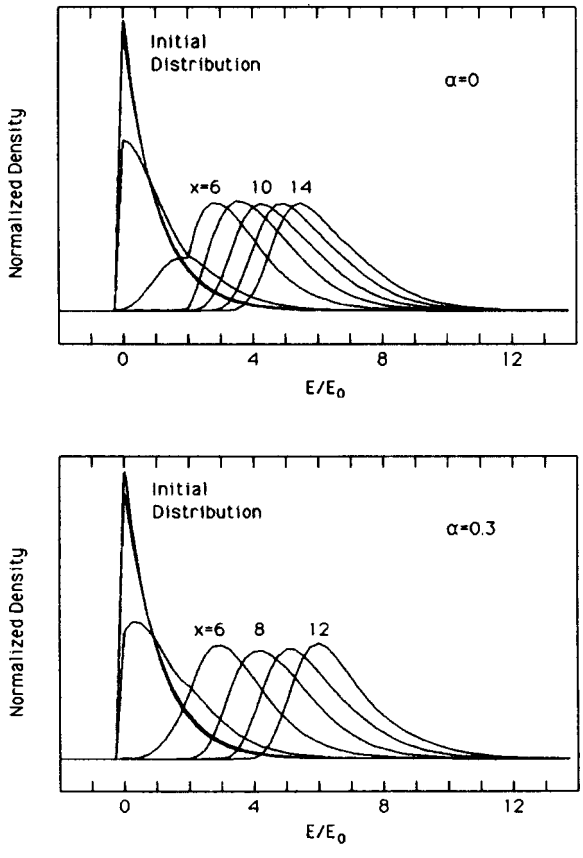

FIG. 13. Computed distribution of carriers trapped in an exponential bandtail as a function of energy measured into the gap for a sequence of time delays $x=\ln(\nu_0 t)$. The initial distribution is assumed to follow the DOS and is therefore also exponential. The upper figure corresponds to $T=0$ while the lower figure is for $\alpha=0.3$.

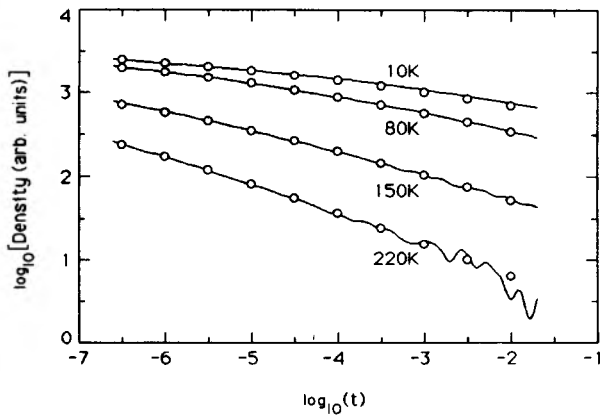

FIG. 14. Comparison of the measured decay (solid lines) of the total number of holes trapped in the valence-band tail to the theoretical decays (open circles) for $T=10$, 80, 150, and 220 K.

correct slopes of the decays are reproduced by the theory as well as their negative curvatures. From the analysis in Sec. V, this latter aspect can only arise if the number of recombination centers remains relatively constant. We were thus correct in assuming this to be true in the experimental time range and using the monomolecular rather than the bimolecular form of the time dependence due to direct tunneling. The persistence of the curvature at 220 K agrees with our theoretical prediction that direct tunneling is important at high temperatures as well as for low temperatures at sufficiently long times following excitation.

It can be concluded that the multiple trapping model which predicts[37] decays of the form $t^{-\alpha}$ is not valid. On the log-log scale of the figure such a power-law decay would appear as a straight line with a negative slope of $\alpha=kT/E_0$. For $T=10$ K and $E_0=46$ meV, the predicted slope is four times smaller than the actual slope at 10 ms.

Further support of the hopping model comes from an examination of the motion of the demarcation energy. MTM predicts[11,12] that when E_d is plotted against logarithmic time, straight lines will result whose slopes are given by kT and whose abcissa intercept is at $\log(t)=-\log(\nu_0)$. According to Fig. 15, this is not the case. There is a substantial shift in E_d even at $T=10$ K and the rate of the shift slows down with time. The same conclusions have been arrived at by Wilson *et al.*[38] for fast PL decays. These features are predicted by the hopping model which reproduces the details of the shifts quite accurately.

C. Dangling bonds

The decay of the effective number of carriers trapped on dangling bonds is compared with the decay of bandtail carriers in Fig. 16. Note that the decay of the DB signal

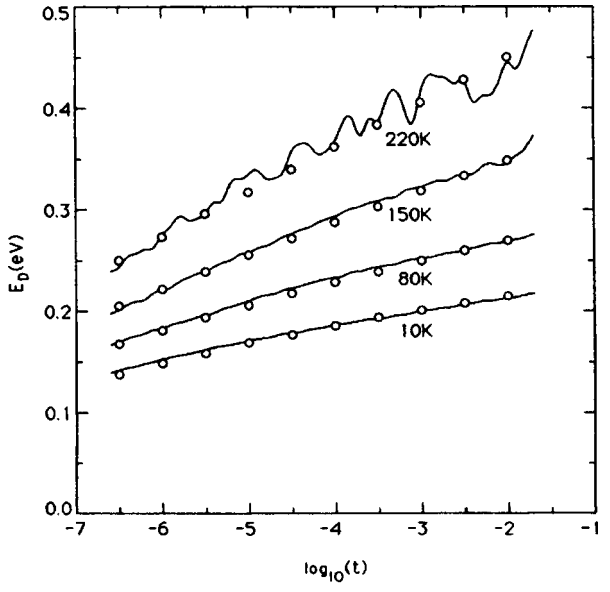

FIG. 15. Comparison of the measured shift (solid lines) in the demarcation energy (E_d) to the theoretical shifts (open circles) for $T=10$, 80, 150, and 220 K.

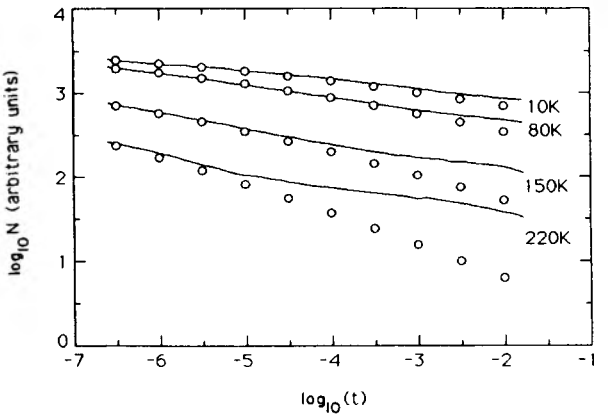

FIG. 16. Comparison of the decay of the dangling bond bands (solid lines) to the measured decay of holes trapped in the bandtail (open circles). The lack of similarity is most pronounced at long times and high temperatures.

is much slower than the decay of the BT signal, especially at long times. We believe that the recombination centers for holes which N_{rc} refers to are predominantly D^- states. The other two possible centers, D^0 and trapped e^- in the conduction-band tail, are negligible by comparison.[1,4,18] One restriction the recombination center must satisfy is that its density remain relatively constant in time. In order for this to be true, either a dynamical balance must be maintained between the two reactions[1]

$$e^-+D^0\rightarrow D^-,\quad e^++D^-\rightarrow D^0\ ,$$

or the number of bandtail carriers is, in the time range of this experiment, small compared to the number of D^- due to early recombination. This monomolecular recombination process is to be contrasted to that of direct recombination between bandtail trapped e^- and e^+ where the reaction is purely bimolecular.[10,18] We note that *linear responses to excitation intensity are not expected even in the monomolecular case due to the dispersion in pair transition rates.* The distribution of these rates is, according to the dependence $\nu(r)=\nu_0 e^{-2r/a}$, determined by the distribution of pair separations[18] which in turn depends nonlinearly on carrier densities. This feature distinguishes the recombination process discussed here from the traditional Shockley-Read treatment.[29]

At sufficiently long times, the population of the bandtails will fall below the equilibrium population of the dangling bonds. The loss of D^- will match that of holes until only D^- and an equal number of D^+ remain. After this time, the final decay of the DB signals is then due to the slow bimolecular reaction $D^++D^-\rightarrow D^0$, which according to Fig. 16, is temperature independent. Direct evidence of this latter process is provided by the 220 K spectra of Fig. 4 which shows only DB absorption and bleaching at long times.

The slowness of this last reaction indicates that D^+ and D^- will not be completely recombined by the time the next excitation pulse arrives (50 ms). After many cycles, a metastable population of charged DB's will be generated.[39] Although this population defines a background

level which is not directly seen in transient measurement, it does cause the observed relative changes in the DB signals to overestimate the relative changes in the total DB population.

At 220 K a shift in the positions (E_1 and E_2) of the positive and negative DB bands towards each other with time is obtained from the fits and is observable in Figs. 4 and 7. This indicates that in addition to recombination, the carriers in D^+ and D^- are thermalizing.

Recombination, as it is understood now, is mediated by D^-. Thus the value of N_{rc} should reflect the number of D^- states. For a typical hole localization radius of 6 Å, $N_{rc}=1.8\times10^{-4}$ gives a D^- concentration of 2.7×10^{17} cm^{-3}. Since the sample, according to its preparation conditions,[21] is expected to have not more than about 5×10^{16} cm^{-3} DB states, this would seem too high. However, the definition of N_{rc} in a more general sense (see Sec. V) is that of an *effective* number of recombination centers per localization volume. It is well known that hole captured by D^- is much faster than by D^0. In fact, values ranging from 5 to 50 have been quoted for the ratio of D^- to D^0 capture cross sections.[4] In the language of the hopping theory of Sec. V, the effective DOS is increased near the charged center by Coulomb attraction. If we assume that recombination is a two-step process in which the rate limiting step is that of electron capture by neutral dangling bonds followed by rapid hole capture on the resultant D^-, then the recombination rates are governed not by hole capture but by the capture of electrons on neutral dangling bonds. Thus, instead of using the hole to D^0 rate as a measure of dangling bond density, one should use the electron to D^0 rate. For an electron radius of 12 Å, a D^0 density of 3.3×10^{16} cm^{-3} is obtained in good agreement with what we had expected. This means that *recombination proceeds via electron capture on D^0 followed by rapid hole capture on the resultant D^-*.

Before concluding this section, it must be pointed out that according to the theory of Sec. V along with the sample parameters presented in this section, saturation of either the conduction- or valence-band tail requires a carrier density in excess of 10^{18} cm^{-3}. Since the excitation flux used in this experiment is held below 10^{14} photons/cm^2, the nonlinear effects arising from state filling have been justifiably ignored. (See Ref. 25 for the results of numerical calculations which obtain the conditions in which saturation is expected.)

VII. PHOTOLUMINESCENCE

In addition to the nonradiative recombination mechanism discussed up to now, there exists a radiative transition between bandtail electrons and holes. It is generally believed that a low temperatures, recombination is dominated by this process.[18] We will now prove that this is not true in our case and that the decay of luminescence agrees exactly with the picture of recombination developed thus far. The reader is referred to the excellent reviews by Street[18] and the works of Dunstan and Boulitrop,[32] and of Wilson *et al.*[38] for further information and alternate opinions.

The additional rate of carrier loss is formally included as the additional term to the master equation

$$d\bar{p}_i/dt=-\sum\overline{p_i w_{ij} n_j}\ , \tag{7.1}$$

where if p_i is interpreted as the probability that state i in the valence tail is occupied by a hole, then n_j is the probability that state j in the conduction tail is occupied by an electron and w_{ij} is that pair radiative transition rate. All luminescence transitions are downwards in energy and have associated with them a fundamental rate of $\nu_r\approx10^8$ sec^{-1} just as nonradiative transitions are characterized by $\nu_0\approx10^{12}$ sec^{-1}.[18] The dependence of w_{ij} on the separation of states is the same as before.

The analysis of the data follows the same strategy as was done for PM. The major difference is the need to include the population distribution of the conduction-band tail as well as the valence-band tail since by (7.1) both are involved.

Assuming that the loss of bandtail carriers is dominated by transitions through defects rather than the radiative process, as will be proven in a moment, the luminescence intensity is given by the ensemble average of (7.1). For spatially random distributions of carriers we obtain in the continuum and infinite volume limit

$$I(E,t)\propto\pi a^3 E\nu_r\int dE' n(E_g-E-E',t)p(E',t)\ , \tag{7.2}$$

where E_g is the energy gap and $n(E,t)$ and $p(E,t)$ are the carrier densities in the conduction- and valence-band tails. Energy is measured in both cases from the band edges into the gap.

The first test is to compare the predicted spectral profiles obtained by (7.2) to the measured spectra ignoring for the moment the decay of the intensity. Using the unnormalized filter functions $H_i(E)$ associated with the $G_i(E)$ described in Sec. II, the relationship between the measured quantities and the actual spectrum is

$$I_i=\int dE\, I(E)H_i(E)\ , \tag{7.3}$$

where I_i is the measured intensity in the ith energy range. Using the previous results for $p(E)$ and the predicted distribution for $n(E)$ given that n_0 is the same as for the valence tail, best fits to the data are obtained using only the conduction-band tail width E_c and the energy gap E_g as variable parameters. The value of E_c obtained in this manner of 26 meV matches exactly the earlier quoted value from the literature.[3] Band gaps may vary by several tenths of an eV depending on sample preparation.[39] The band-gap value of $E_g=1.65$ eV agrees with 1.64 eV obtained using photothermal deflection spectroscopy on similarly prepared samples.[21]

The most interesting information is contained in the time dependences of the whole-band PL decays. If the assumption that recombination is governed by the nonradiative recombination mechanism is correct, then the decay derived from integration of $I(E,t)$ over energy should, aside from a scaling constant, match the observed total PL decay. On the other hand, if recombination is

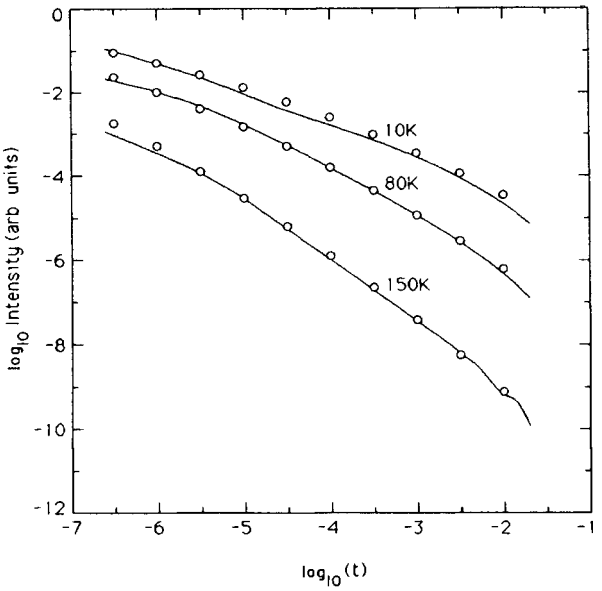

FIG. 17. Comparison of theory to the measured whole-band PL decays at 10, 80, and 150 K assuming nonradiative dominated recombination. The solid lines are the experimental results and the circles correspond to the calculated decays.

dominated by the radiative transition itself, the time derivative of the hole decay will be proportional to the luminescence intensity. Using the information already obtained about the decay of holes, and taking the decay of electrons to have the same time dependence, excellent fits were obtained to the data at all temperatures. See Fig. 17 for graphs of both measured and predicted decays. On the other hand, when the derivative of hole decay is used, the agreement is rather poor as indicated by Fig. 18. Thus, even at 10 K where the luminescence efficiency is highest, recombination in our sample is still controlled by the nonradiative process. This is not at all an unreasonable result. The highest reported luminescence efficiency obtained using a very strong excitation intensity of 70 mW/cm^2 is 19±10 %.[35] Lack of correlation between PL and carrier decay has been reported before.[40]

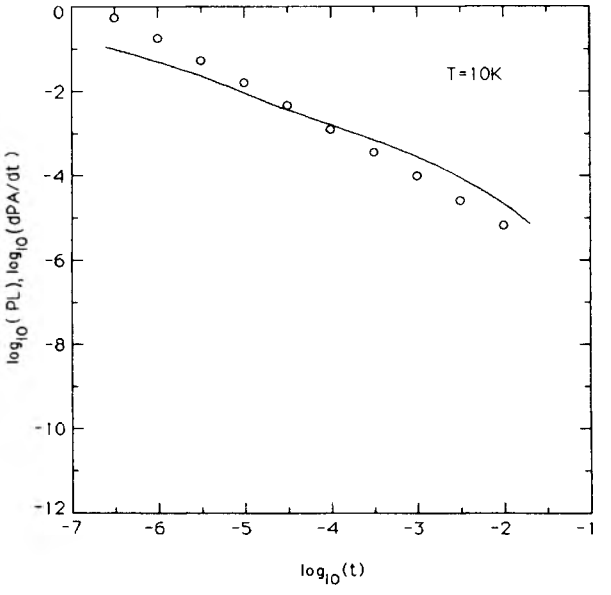

FIG. 18. Comparison of the time derivative of the total bandtail PM signal to the decay of whole-band PL at 10 K. The solid lines are the experimental results and the circles correspond to the calculated decays. If radiative recombination dominated, these curves would be the same.

VIII. SUMMARY

We have constructed a new apparatus of sufficient sensitivity to allow for the measurement of spectrally resolved transient PA over five decades in time. Application of this technique to undoped *a*-Si:H has yielded detailed information concerning the distribution of excess carriers trapped within the gap.

In addition to the observation of holes trapped in the valence-band tail, carriers trapped on dangling bonds have been identified. The distinguishing features of these states are a high-energy onset and a slow decay. A positive aborption onset associated with the transition of electrons from D^- to the conduction band is observed at 0.65 eV. A bleaching onset located at 1.08 eV into the gap, whose strength relative to the absorption signal is constant with time, is ascribed to the loss of D^0 states upon conversion to D^- by fast electron capture which would otherwise have produced a positive absorption signal in the dark. The number of excess D^-, and hence diminished D^0 is determined by the relative capture rates of electrons and holes on D^0 and D^-, respectively. The 0.43-eV energy difference between these onsets gives the effective correlation energy of the dangling bonds.

A theoretical description of carrier thermalization and recombination based on bandtail hopping has been derived which, in a unified manner, takes into account thermally activated hopping as well as direct tunneling. The temperature-dependent analytical solutions for the total decay of bandtail carriers and their shift in energy agree with existing models in the temperature regimes for which the models are valid. Numerically computed distributions of bandtail carriers in time, temperature, and energy have been obtained and used to fit the spectral dependence of our data. The additional mechanism of a two-step recombination process involving dangling bonds as the intermediate states has been included in our analysis in order to obtain total agreement with the measured time dependence of the decays. Thus a complete picture of carrier relaxation is obtained. Furthermore, the parameters of the theory involve physical quantities which have been measured elsewhere. The values of these parameters which best fit our data are in excellent agreement with accepted values.

We have also measured spectrally resolved transient photoluminescence. The number and distribution of electrons in the conduction-band tail has been calculated based on the above recombination-thermalization model using experimental information obtained regarding

bandtail holes. The spectrum and decay of the measured luminescence intensity is in agreement with that predicted from the deduced joint density of bandtail carriers. The time dependence of the intensity decay does not fit the PA data when it is assumed that direct tail-to-tail recombination dominates.

ACKNOWLEDGMENTS

We thank W. Paul and R. A. Street for the samples and T. R. Kirst for technical assistance. The work was partly supported by National Science Foundation (NSF) Grant No. DMR-82-09148.

---

*Present address: Department of Physics, University of Utah, Salt Lake City, UT 84112.

[1]R. A. Street, D. K. Biegelsen, and R. L. Weisfield, Phys. Rev. B **30**, 5861 (1984).

[2]B. A. Wilson, P. Hu, T. M. Jedju, and J. P. Harbison, Phys. Rev. B **28**, 5901 (1983).

[3]T. Tiedge, T. M. Cebulka, D. L. Morse, and B. Abeles, Phys. Rev. Lett. **46**, 1425 (1981).

[4]R. A. Street, Appl. Phys. Lett. **41**, 1060 (1982).

[5]R. Pandya, E. A. Schiff, and K. A. Conrad, J. Non-Cryst. Solids **66**, 193 (1984).

[6]F. Boulitrop, Phys. Rev. B **28**, 6192 (1983).

[7]J. Tauc, in *Hydrogenated Amorphous Silicon, Semiconductors and Semimetals,* edited by J. Pankove (Academic, New York, 1984), Vol. 21B, p. 299.

[8]J. Tauc and Z. Vardeny, Philos. Mag. B **52**, 313 (1985).

[9]P. O'Connor and J. Tauc, Phys. Rev. B **25**, 2748 (1982).

[10]Z. Vardeny, P. O'Conner, S. Ray, and J. Tauc, Phys. Rev. Lett. **44**, 1267 (1980); **46**, 1108 (1981).

[11]T. Tiedje and A. Rose, Solid State Commun. **37**, 49 (1980).

[12]J. Orenstein and M. A. Kastner, Phys. Rev. Lett. **46**, 1421 (1981).

[13]D. Monroe, Phys. Rev. Lett. **54**, 146 (1985).

[14]K. Maschke, E. Merk, and W. Czaja, Helv. Phys. Acta. **58**, 417 (1985).

[15]S. Ray, Z. Vardeny, and J. Tauc, J. Phys. (Paris) Colloq. **42**, C4-555 (1981); *Tetrahedrally Bonded Amorphous Semiconductors (Carefree, 1981),* Proceedings of a Topical Conference on Tetrahedrally Bonded Amorphous Semiconductors, AIP Conf. Proc. No. 73, edited by R. A. Street, D. K. Biegelson, and J. C. Knights (AIP, New York, 1981), p. 253.

[16]D. Pfost, Z. Vardeny, and J. Tauc, Phys. Rev. Lett. **52**, 376 (1984).

[17]D. Pfost, Z. Vardeny, and J. Tauc, Phys. Rev. B **30**, 1083 (1984).

[18]R. A. Street, Adv. Phys. **30**, 593 (1981).

[19]F. Boulitrop, J. Dijon, D. J. Dunstan, and A. Herve, in *Proceedings of the 17th International Conference on the Physics of Semiconductors,* edited by J. D. Chadi and W. A. Harrison (Springer-Verlag, Berlin, 1984), p. 873.

[20]Z. Vardeny and J. Tauc, Phys. Rev. Lett. **54**, 1844 (1985).

[21]G. D. Cody, B. G. Brooks, and B. Abeles, Solar Energy Mater. **8**, 231 (1982).

[22]J. Kočka, J. Non-Cryst. Solids **90**, 91 (1987).

[23]H. Dersch, J. Stuke, and J. Beichler, Phys. Status Solidi **105**, 265 (1981).

[24]W. B. Jackson, Solid State Commun. **44**, 477 (1982).

[25]H. A. Stoddart, Ph.D. thesis, Brown University, 1987 (unpublished).

[26]M. Silver, G. Schoenherr, and H. Baessler, Phys. Rev. Lett. **48**, 352 (1982).

[27]F. Reif, *Fundamentals of Statistical and Thermal Physics* (McGraw-Hill, New York, 1965), p. 552.

[28]D. G. Thomas, J. J. Hopfield, and W. M. Augustyniak, Phys. Rev. **140**, A202 (1965).

[29]W. Shockley and W. T. Read, Phys. Rev. **87**, 835 (1952).

[30]D. Wake and N. Amer, Phys. Rev. B **27**, 2598 (1983).

[31]D. J. Dunstan, Philos. Mag. B **46**, 579 (1982); Solid State Commun. **43**, 341 (1982); Philos. Mag. B **49**, 191 (1984).

[32]D. J. Dunstan and F. Boulitrop, Phys. Rev. B **30**, 5945 (1984).

[33]C. Tsang and R. A. Street, Phys. Rev. B **19**, 3027 (1979).

[34]W. B. Jackson and R. J. Nemanich, J. Non-Cryst. Solids **59&60**, 353 (1983).

[35]S. Griep and L. Ley, J. Non-Cryst. Solids **59&60**, 253 (1983).

[36]C. B. Roxlo, B. Abeles, C. R. Wronski, G. D. Cody, and T. Tiedje, Exxon Corporate Research Report, 1982 (unpublished).

[37]J. Orenstein and M. A. Kastner, Solid State Commun. **40**, 85 (1981).

[38]B. A. Wilson, T. P. Kerwin, and J. P. Harbison, Phys. Rev. B **31**, 7953 (1985).

[39]G. D. Cody, T. Tiedge, B. Abeles, B. Brooks, and Y. Goldstein, Phys. Rev. Lett. **47**, 1480 (1981).

[40]T. M. Searle, T. S. Nashashibi, I. G. Austin, R. Devonshire, and G. Lockwood, Philos. Mag. B **39**, 389 (1979).

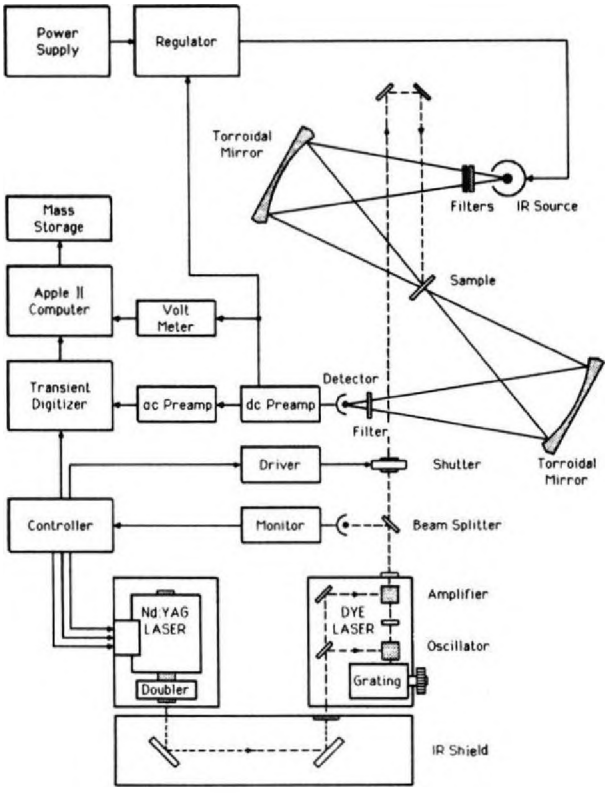

FIG. 1. Block diagram of the experimental apparatus.